Anomalous photobleaching in fluorescence recovery after photobleaching measurements due to excitation saturation—a case study for fluorescein

Kevin Braeckmans
Barbara G. Stubbe
Katrien Remaut
Joseph Demeester
Stefaan C. De Smedt
Ghent University
Laboratory of General Biochemistry and Physical Pharmacy
Harelbekestraat 72
9000 Ghent, Belgium
E-mail: stefaan.desmedt@ugent.be

Abstract. In this study we examine the implications of excitation saturation on fluorescence recovery after photobleaching (FRAP) experiments. In particular we present both experimental and theoretical evidence that fluorescein, one of the most frequently used fluorophores in FRAP, does not always comply with the basic assumptions that are made in many FRAP models: an invariant bleaching illumination intensity distribution (BID) in combination with first-order photobleaching kinetics. High light intensity levels, which are typical for the photobleaching phase of FRAP experiments, can cause excitation saturation of fluorescein in the excited triplet state. We show by experiments and computer simulations that under such saturating conditions the higher-order diffraction maxima of the BID substantially contribute to the photobleaching process and can no longer be neglected. As a result, the bleached regions are larger than expected theoretically from the FRAP models. Although this effect is not always directly evident from the FRAP experiments, neglecting it may shift the calculated diffusion coefficient by as much as over one order of magnitude. We present a discussion on the implications of this saturation effect on various types of FRAP models. [DOI: 10.1117/1.2337531]

Keywords: photobleaching; saturation; fluorescein; fluorescence recovery after photobleaching; confocal scanning laser microscopy; diffusion.

Paper 05390R received Dec. 23, 2005; revised manuscript received Mar. 16, 2006; accepted for publication Apr. 19, 2006; published online Aug. 25, 2006.

1 Introduction

A well-known, yet ever-evolving fluorescence technology that is used for measuring the mobility of molecules on a microscopic level is fluorescence recovery after photobleaching (FRAP).[1–3] Basically, the fluorescent molecules are at first photobleached in a certain region of the sample and immediately after the bleaching phase, fluorescent molecules from the surrounding unbleached areas will start to diffuse into the bleached area. The resulting recovery of the fluorescence in the bleached area is subsequently measured by a highly attenuated light beam. The rate of fluorescence recovery reflects the mobility of the species in the system, expressed by the effective translational diffusion coefficient D. FRAP has been used, for example, in cellular applications to assess the translational mobility of all kinds of solutes in cytoplasm, nuclei, and membranes[3–7] and extracellular matrices such as cervical mucus, biofilms, cystic fibrosis sputum, and bovine vitreous.[8–11]

The diffusion coefficient can be calculated from a FRAP experiment by fitting of an appropriate FRAP model to the experimental recovery curve. In many FRAP models—the so-called discontinuous photobleaching techniques—the bleaching phase is assumed to be very short compared to the recovery time.[11–20] Consequently, diffusion during bleaching can be neglected and the bleaching phase can be solely described by the photochemical bleaching process. In addition, the assumption is usually made that the bleaching process can be described by an irreversible first-order reaction:[11–13,15–18,21–23]

$$\frac{\partial C(x,y,z,t)}{\partial t} = -\alpha I_b(x,y,z)C(x,y,z,t), \tag{1}$$

where $C(x,y,z,t)$ is the spatial concentration distribution of fluorophores at a time t, α is the bleach rate, which is specific for a specific fluorophore in a particular medium, and $I_b(x,y,z)$ is the bleaching illumination intensity distribution (BID). Equation (1) is based on the simple reaction scheme of fluorophore + photon → photobleaching product. If the bleaching beam is stationary, Eq. (1) immediately leads to

$$C_b(x,y,z) = C_0(x,y,z)e^{-\alpha I_b(x,y,z)t}, \tag{2}$$

where $C_0(x,y,z)$ is the fluorophore concentration distribution before bleaching and $C_b(x,y,z)$ the fluorophore concentration distribution after bleaching during a time t. In case of a ge-

Address all correspondence to Stefaan De Smedt, Lab General Biochemistry and Physical Pharmacy, Ghent University, Harelbekestraat 72, Ghent, 9000 Belgium; Tel: +32 9 264.80.76; Fax: +32 9 264.81.89; E-mail: stefaan.desmedt@ugent.be

1083-3668/2006/11(4)/044013/13/$22.00 © 2006 SPIE

ometry being bleached by a scanning beam, which is mostly the case for FRAP experiments on a CSLM, Eq. (1) leads to[11]

$$C_b(x,y,z) = C_0(x,y,z)e^{-\alpha I/(v\Delta y)K(x,y,z)}, \tag{3}$$

where v is the line scanning speed and Δy the distance between two adjacent scanning lines and where it is understood that Δy is smaller than half the resolution of the BID. $K(x,y,z)$ is the bleaching illumination intensity distribution that results from scanning the area $B(x,y)$ with the BID $I_b(x,y,z)$ and can be calculated from their convolution product:

$$K(x,y,z) = B(x,y) \otimes I_b(x,y,z) = \int_{-\infty}^{+\infty}\int_{-\infty}^{+\infty} B(x',y')I_b(x-x',y-y',z)dx'dy'. \tag{4}$$

After the instantaneous photobleaching phase, the fluorescence inside the bleached region will gradually recover due to diffusion of the bleached fluorophores out of the bleached region and diffusion of unbleached fluorophores from the surroundings into the bleached region. The diffusion process is described by Fick's second law:[24]

$$\frac{\partial}{\partial t}C(x,y,z,t) = D\nabla^2 C(x,y,z,t), \tag{5}$$

where D (m^2/s) is the diffusion coefficient and $C(x,y,z,t)$ the spatial concentration distribution of the diffusing substance at a time t after bleaching. To model the recovery phase, this differential equation has to be solved for the concentration distribution right after bleaching as calculated from Eq. (2) or (3). Hence, the correctness of the FRAP model depends directly on the validity of assuming first-order kinetics for the photobleaching process. In case first-order kinetics are not valid, the concentration distribution after bleaching will be different from the one calculated from Eq. (2) or (3). Consequently, the FRAP model will no longer be valid, leading to incorrectly calculated values for the diffusion coefficient.

A very popular fluorophore for FRAP is fluorescein[1,3] because it photobleaches easily and therefore can comply with the assumption of a very short bleaching phase. It has been shown, however, that the bleaching process of fluorescein is not a simple first-order reaction and in microscopy, in general, it does not follow a single exponential decay.[25] It is therefore to be expected that the concentration distribution after bleaching is generally no longer accurately predicted by Eqs. (2) and (3) when using fluorescein, especially under the saturating conditions of the photobleaching phase.

Here we study the effect of excitation saturation of fluorescein on the concentration distribution after photobleaching. First we will repeat in short the photochemical processes leading to the photobleaching of fluorescein. Then we will examine in detail, both experimentally and theoretically, the concentration distribution of fluorescein after photobleaching with the confocal microscope as a function of the bleaching light intensity. Finally, a discussion will be given on the implications of excitation saturation on various FRAP models.

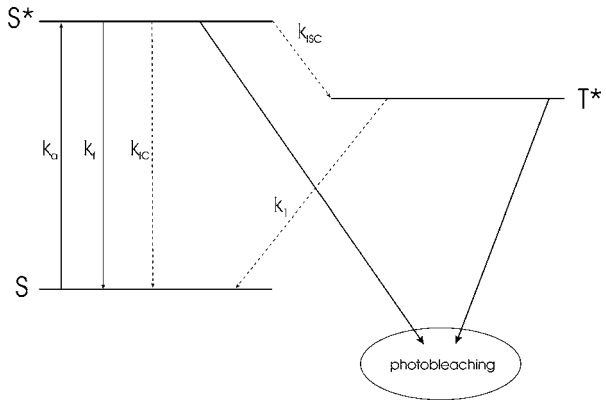

Fig. 1 A simplified Jablonski energy diagram for a typical fluorophore showing possible transitions between the ground state S, the excited singlet state S^*, and the excited triplet state T^*, as explained in the main text.

2 Theoretical Background: Photobleaching of Fluorescein in Microscopy

2.1 *The Photobleaching Process of Fluorescein*

A detailed description of the photobleaching kinetics of fluorescein has been published by Song et al.[25] As the photobleaching process in the computer simulations of this study is based on the work of Song et al., we will repeat the main conclusions here for convenience of the reader. A fluorophore can make an electronic transition from the ground state S to the excited singlet state S^* (see Fig. 1) by absorbing a photon of wavelength λ (m) and corresponding energy hc/λ_{ex}, where h is Planck's constant and c is the speed of light. If the excitation light has an irradiance H (W/m^2) and the fluorophore has an absorption cross-section σ_a (m^2/molecule), the rate of photon absorption k_a (s^{-1}) is

$$k_a = \sigma_a\left(H \cdot \frac{\lambda_{ex}}{hc}\right), \tag{6}$$

The absorption cross-section for fluorescein at 488 nm and pH$>$7 is 3.06×10^{-20} m^2/molecule.[26] The number of fluorophores in the excited singlet state S^* will be depopulated via fluorescence emission (rate k_f), radiationless internal conversion (rate k_{ic}), and radiationless intersystem crossing to the excited triplet state T^* (rate k_{isc}). The spin-forbidden transition from T^* to S will happen at a (usually very low) rate k_1. While being in the excited singlet or triplet state, irreversible photochemical destruction of the fluorophores can occur, a process termed *photobleaching*. Those fluorophores that are photobleached can no longer take part in the fluorescence excitation-emission cycle.

For fluorescein it has been demonstrated that the short-lived excited singlet state does ordinarily not contribute to the photobleaching mechanism. The long-lived triplet excited state, at the other hand, becomes depopulated via two major pathways: (1) the reaction between a triplet and another triplet or a ground state fluorescein molecule, and (2) the reaction between a triplet fluorescein molecule and an oxygen molecule. These two mechanisms are termed the dye-to-dye (D-D) and dye-to-oxygen (D-O) mechanisms and can lead to

Table 1 Photochemical reactions of fluorescein.

Reaction	Description	Rate constants
$S + h\nu \rightarrow S^*$	Photon absorption	k_a
$S^* \rightarrow S + h\nu'$	Fluorescence emission	$k_d = k_f + k_{IC} = 2.134 \times 10^8\ s^{-1}$
$S^* \rightarrow S$	Internal conversion	
$S^* \rightarrow T^*$	Intersystem crossing	$k_{isc} = 6.6 \times 10^6\ s^{-1}$
$T^* \rightarrow S$	Radiationless deactivation	$k_1 = 50\ s^{-1}$
$T^* + T^* \rightarrow T^* + S$	Triplet quenching	$k_2 = 5 \times 10^8\ M^{-1}\ s^{-1}$
$T^* + S \rightarrow S + S$	Triplet quenching	$k_3 = 5 \times 10^7\ M^{-1}\ s^{-1}$
$T^* + T^* \rightarrow R + X$	Electron transfer	$k_4 = 6 \times 10^8\ M^{-1}\ s^{-1}$
$T^* + S \rightarrow R + X$	Electron transfer	$k_5 = 5 \times 10^7\ M^{-1}\ s^{-1}$
$T^* + X \rightarrow S + X$	T^* quenching by X	$k_6 + k_7 = 5 \times 10^8\ M^{-1}\ s^{-1}$
$T^* + R \rightarrow S + R$	T^* quenching by R	
$T^* + O_2 \rightarrow S + O_2$	Physical quenching by O_2	$k_8 = 1.56 \times 10^9\ M^{-1}\ s^{-1}$
$T^* + O_2 \rightarrow X + HO_2$ (or O_2^-)	Chemical quenching by O_2	$k_9 = 1.4 \times 10^8\ M^{-1}\ s^{-1}$

Reproduced from Song et al.[25]

either reduced (R) or semi-oxidized (X) radical forms. These radicals can again react with triplet state molecules and revert either to stable nonfluorescent photoproducts or back to the ground state. Song et al.[25] have incorporated all relevant photochemical reactions into a theoretical model comprising the following six coupled differential equations:

$$\frac{d}{dt}[N_S(t)] = [k_d N_{S^*}(t) + k_1 N_{T^*}(t) + k_2 N_{T^*}^2(t) + k_3 N_{T^*}(t) N_S(t) + k_6 N_{T^*}(t) N_X(t) + k_7 N_{T^*}(t) N_R(t) + k_8 N_{T^*}(t) N_{O_2}(t)] - [k_a N_S(t) + k_5 N_{T^*}(t) N_S(t)],$$

$$\frac{d}{dt}[N_{S^*}(t)] = k_a N_S(t) - [k_d N_{S^*}(t) + k_{isc} N_{S^*}(t)],$$

$$\frac{d}{dt}[N_{T^*}(t)] = k_{isc} N_{S^*}(t) - [k_1 N_{T^*}(t) + k_2 N_{T^*}^2(t) + k_3 N_{T^*}(t) N_S(t) + 2k_4 N_{T^*}^2(t) + k_5 N_{T^*}(t) N_S(t) + k_6 N_{T^*}(t) N_X(t) + k_7 N_{T^*}(t) N_R(t) + k_8 N_{T^*}(t) N_{O_2}(t) + k_9 N_{T^*}(t) N_{O_2}(t)],$$

$$\frac{d}{dt}[N_X(t)] = k_4 N_{T^*}^2(t) + k_5 N_{T^*}(t) N_S(t) + k_9 N_{T^*}(t) N_{O_2}(t),$$

$$\frac{d}{dt}[N_R(t)] = k_4 N_{T^*}^2(t) + k_5 N_{T^*}(t) N_S(t),$$

$$\frac{d}{dt}[N_{O_2}(t)] = -k_9 N_{T^*}(t) N_{O_2}(t). \quad (7)$$

The individual photochemical reactions and the corresponding rate constants as reported in Song et al.[25] are shown in Table 1. This set of differential equations has to be solved numerically for a given rate of photon absorption k_a and initial values for the concentrations N_S, N_{S^*}, N_{T^*}, N_X, N_R, and N_{O_2}. The rate of photon absorption k_a can be calculated from Eq. (6) for a given irradiance H.

2.2 *Photobleaching of Fluorescein by a Focused Laser Beam*

When a laser beam is focused down through an objective lens, a complex 3-D intensity distribution results around the focal point. For clarity and because most FRAP models are limited to diffusion in two dimensions, the study presented here will be restricted to two dimensions as well (focal plane). The conclusions from this study equally apply to the third dimension as well. The radial irradiance distribution in the focal plane of a (confocal) microscope's objective lens is in good approximation given by the Fraunhofer–Airy formula, which is valid for small diffraction angles:[27–29]

$$H(r) = P\pi\left(\frac{0.61}{w}\right)^2\left[\frac{2J_1(1.22\pi r/w)}{1.22\pi r/w}\right]^2, \quad (8)$$

where P is the power (W) of the light emerging from the objective lens, J_1 is the first-order Bessel function of the first kind, and w the resolution of the lens, which is defined as the position of the first minimum. For an objective lens of numerical aperture NA, the resolution can be calculated from the

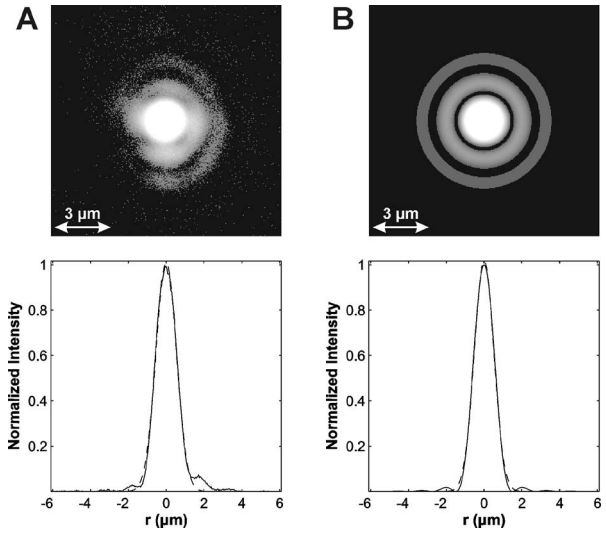

Fig. 2 The illumination intensity distribution in the focal plane. (a) The diffraction pattern in the focal plane of the 10× objective lens has been recorded by imaging a 190-nm fluorescent nanosphere with the confocal microscope. The confocal diaphragm was opened completely to allow the light coming from higher-order diffraction rings to enter the detector. Besides the central maximum, the first- and second-order diffraction rings are visible as well after applying a logarithmic color map. The intensity distribution along the vertical direction in the image is also shown (solid line). The central peak can be very well approximated by a Gaussian intensity distribution (dashed line). (b) For comparison, the diffraction pattern according to the Fraunhofer–Airy formula is shown as well using the same color map. Again the central peak of the theoretical curve (solid line) can be very well approximated by a Gaussian intensity distribution (dashed line).

Rayleigh criterion:[30] $w=0.61\lambda/\mathrm{NA}$. Figure 2(a) shows the actual diffraction pattern in the focal plane of the objective lens that will be used in this study (see "Materials"), which is recorded by imaging a small fluorescent nanosphere with a completely opened confocal diaphragm. A logarithmic colormap was applied to make the first- and second-order diffraction rings visible. Since the real diffraction pattern is not perfectly radially symmetric, most likely due to slight imperfections of the microscope's optical path, we will show throughout this study the intensity profiles along one direction only (y-direction). The intensity distribution along the y-direction is shown in Fig. 2(a). By analyzing the position of the first minimum, we find that the resolution w is approximately 1.5 μm. For comparison, the theoretical irradiance distribution according to Eq. (8) is shown in Fig. 2(b) for $w=1.5$ μm. As expected, Eq. (8) adequately represents the diffraction pattern of the focused laser beam at the focal plane.

For most fluorescence applications it is sufficient to take the central part of the diffraction pattern into account. For example, the central peak of the Fraunhofer–Airy distribution contains 84% of the total amount of light in the diffraction pattern while the subsequent higher-order maxima have a relative intensity of only 1.7%, 0.4%, 0.1%, etc. Hence, also for FRAP models a more simple Gaussian distribution is ordinarily used to describe the BID:

$$H(r) = H(0)e^{-2r^2/r_0^2}, \tag{9}$$

which accurately describes the central peak as is shown by the best fit of Eq. (9) in Figs. 2(a) and 2(b). In that context, the parameter r_0 is usually referred to as the resolution of the BID as well, but differs slightly from w because it has a different definition [$r_0 \approx 0.69w$, as determined by a best fit of Eq. (9) to Eq. (8)].

FRAP models that explicitly take the BID into account never use the relatively complicated Eq. (8) but rather the simplified Gaussian intensity distribution Eq. (9)[2,16–18,21] or possibly a 3-D extension with an additional axial (modified) Gaussian distribution.[11,15,23] However, as we will show further on, the higher-order diffraction maxima cannot be neglected any longer in case of fluorescein being bleached by a high-intensity laser beam. Under the extreme illumination conditions of the bleaching phase, even the higher-order diffraction maxima will be able to populate the excited triplet state T^* significantly, resulting in a complex expanded bleaching profile that can no longer be explained by simple first-order photobleaching with a Gaussian intensity distribution.

3 Materials and Methods

3.1 *The Bleaching and Imaging System*

The FRAP experiments are performed on a CSLM (model MRC1024 UV, Bio-Rad, Hemel Hempstead, UK) equipped with the SCAMPER module for photobleaching experiments.[31,32] The module consists of a 4 W Ar-ion laser (model Stabilite 2017; Spectra-Physics, Darmstadt, Germany) and an acousto-optical modulator (AOM) (Brimrose, Campbell, Baltimore, MD, USA), controlled by a computer and dedicated software. The AOM controls the intensity of the laser beam that is sent to the CSLM. A high-power laser beam ("bleaching beam") is used for photobleaching, while a low-power beam ("detection beam") is used for the recording of the confocal images. Bleaching masks can be designed in the software that controls the AOM. While recording an image with the CSLM, low- and high-power laser light is sent to the sample according to the selected bleaching mask.

All bleaching experiments have been performed with the 488-nm line from the Ar-ion laser. The intensity of the laser beam at the sample can be controlled over a range of 0 to 10 mW. A 10× objective lens (CFI Plan Apochromat; Nikon, Badhoevedorp, The Netherlands) with a numerical aperture (NA) of 0.45 was used for bleaching. On the Bio-Rad confocal microscope, the back aperture of this lens is only partially filled, however, resulting in a lower effective NA of about 0.2 for the illumination beam and a corresponding resolution $w=1.5$ μm (and $r_0=1.0$ μm). The resolution was determined by directly imaging 190-nm fluorescent nanospheres (Molecular Probes, Leiden, The Netherlands) with a completely opened confocal diaphragm. Imaging of the bleached profiles was done with a high-resolution 60× water immersion lens of 1.2 NA (CFI Plan Apochromat; Nikon, Badhoevedorp, The Netherlands) having a resolution w of approximately 0.25 μm.

3.2 *Photobleaching Experiments*

Fluorescein isothiocyanate dextrans (Sigma-Aldrich, Bornem, Belgium) of 2000 kDa molecular weight (FD2000) were incorporated in an acrylamide gel. The acrylamide gel was prepared by radical polymerization of an aqueous acrylamide solution (30% w/w). The solution was prepared by dissolving

acrylamide in deoxygenated phosphate buffer (10 mM Na_2HPO_4, 0.02% sodium-azide, adjusted with 1 N hydrochloric acid to pH 7.0). Prior to addition of the gelation reagents, 3.915 mg/g gel of FD2000 was added. The polymerization reagents were N,N,N′,N′-tetramethylene-ethylenediamine (TEMED; Fluka, Buchs, Switzerland) and ammonium persulphate (10% w/v) (APS; VWR International, Leuven, Belgium). The procedure involves adding 0.5 μL TEMED solution to 1 g hydrogel. After mixing, 2.5 μL APS solution was added to initiate gelation. The gelating mixture was transferred into a cuvette with a glass bottom for use with an inverted microscope (Nalge Nunc International, Naperville, IL, USA). The gelation required 1 hour at room temperature. FRAP measurements using the CSLM[11] revealed a very low diffusion coefficient of 0.020 ± 0.005 $\mu m^2/s$ and a large fraction of immobile fluorescent FITC-dextrans of $90\pm5\%$.

Bleaching experiments were performed with a stationary laser beam ("beam parked") or a line scanning beam. The laser power at the sample was between 1 μW and 5 μW for imaging and up to 10 mW for bleaching. The time between the bleaching phase and imaging of the bleached profiles was approximately 30 min to allow diffusion of the (small) mobile fraction to complete. After that time, the remaining bleached profile is due to the immobile fraction and reflects directly the bleaching profile immediately after bleaching. Confocal images of the bleaching profiles were recorded with the 60 $\times$ 1.2 NA objective lens to obtain the best possible resolution. Before normalizing the confocal images to the background fluorescence (i.e., unbleached fluorophores), they were convolved with a median smoothing mask to reduce the noise.

3.3 *Photobleaching simulations*

To study the bleaching of fluorescein at the focal plane, a computer program was written to solve the six coupled differential Eqs. (7) numerically. For the simulation of the spot photobleaching experiments, the absorption rate $k_a(r)$ is calculated from Eqs. (6) and (8). At first a set of radial coordinates r is defined (the spatial mesh) together with the initial concentrations of N_S, N_{S^*}, N_{T^*}, N_X, N_R, and N_{O_2}. In the simulations reported here, it is always assumed that all fluorescein molecules are initially in the ground state ($N_{S^*}=N_{T^*}=N_X=N_R=0$). Next, the differential equations are solved for each of the radial coordinates and the corresponding value of $k_a(r)$. When the illumination time t has passed, in general there still will be a number of fluorescein molecules in the excited singlet and triplet state: N_{S^*} & $N_{T^*}>0$. Therefore, even when the illumination is switched off, the photobleaching reactions still can go on for some time until all the molecules are either bleached or back in the ground state. This has been taken into account in the simulation program by setting k_a to zero after the bleaching time t and continue to solve the differential equations until the number of bleached molecules (N_X+N_R) together with the number of ground state molecules N_S are equal to the initial number of molecules.

In FRAP experiments on the CSLM, a scanning beam is often used for bleaching rather than a stationary beam.[11,17,23,32–36] Therefore, the program for the simulation of the photobleaching of fluorescein was extended for a line-scanning beam as well. When bleaching a line segment, the bleaching will be uniform along the scanning direction (except at the beginning and the end of the line). Only in the direction perpendicular to the scanning direction a bleaching gradient will exist. It is therefore sufficient to calculate the bleaching profile perpendicular to the scanning direction for one position on the bleached line segment only. In the simulation algorithm, the line scanning is taken into account by first defining a start and end position of the laser beam (x_s and x_e) relative to the position on the line at which the bleaching profile is calculated (x_0): the laser beam starts at position x_s and is moved at a scanning speed ν in discrete steps Δx toward the position x_e. At each step the laser beam is stationary for a time $\Delta t=\Delta x/\nu$ and the effect is calculated at position x_0. The smaller the step size Δx, the better the continuous movement of the laser scanning beam will be approximated (at the cost of an increased calculation time). All line scanning simulations reported here were calculated with a step size that is one fifth of the resolution of the bleaching beam ($\Delta x=w/5$) since no appreciable differences in the calculated bleaching profiles were observed for smaller step sizes. The start and end positions of the bleaching beam were always taken symmetrically at 10 times the resolution of the bleaching beam: $x_s=x_0-10w$ and $x_e=x_0+10w$.

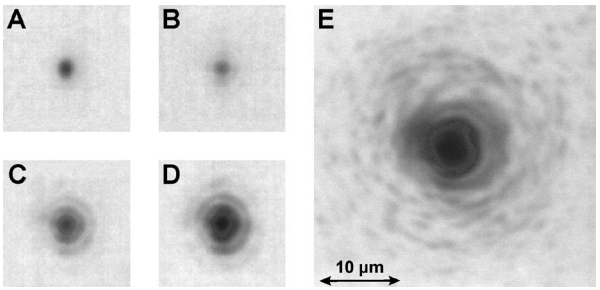

Fig. 3 Using a stationary laser beam, spots are photobleached in an acrylamide gel loaded with FITC-dextrans. All images are shown to the same scale. (a) At a low intensity of 2 μW and a bleaching time of 125 ms, only the central peak of the BID contributes to the bleaching process. (b) At a high bleaching intensity of 10 mW and a bleaching time of 100 μs, also the first-order diffraction ring is able to cause photobleaching. (c) For a bleaching time of 500 μs and (d) 1000 μs at 10 mW, the contribution of the first and second diffraction ring is becoming even more pronounced. (e) When increasing the illumination time to 100 ms, the fourth diffraction ring is clearly showing up as well, together with various diffraction spots. The square root of the original image is displayed here for better visibility of all features.

4 Results

4.1 *Photobleaching of Immobilized FD2000*

To visualize the bleaching profiles at different bleaching conditions, FITC-dextrans of molecular weight 2000 kDa were incorporated into an acrylamide gel. Using a stationary laser beam, spots were photobleached in the gel with a low NA objective lens for different bleaching times. Confocal images were subsequently recorded using a high NA objective lens to obtain the best possible resolution. Some examples are shown in Fig. 3.

To be able to relate the results of this study directly to the existing FRAP models (see Discussion), we will now define the "apparent BID" as the intensity distribution one would

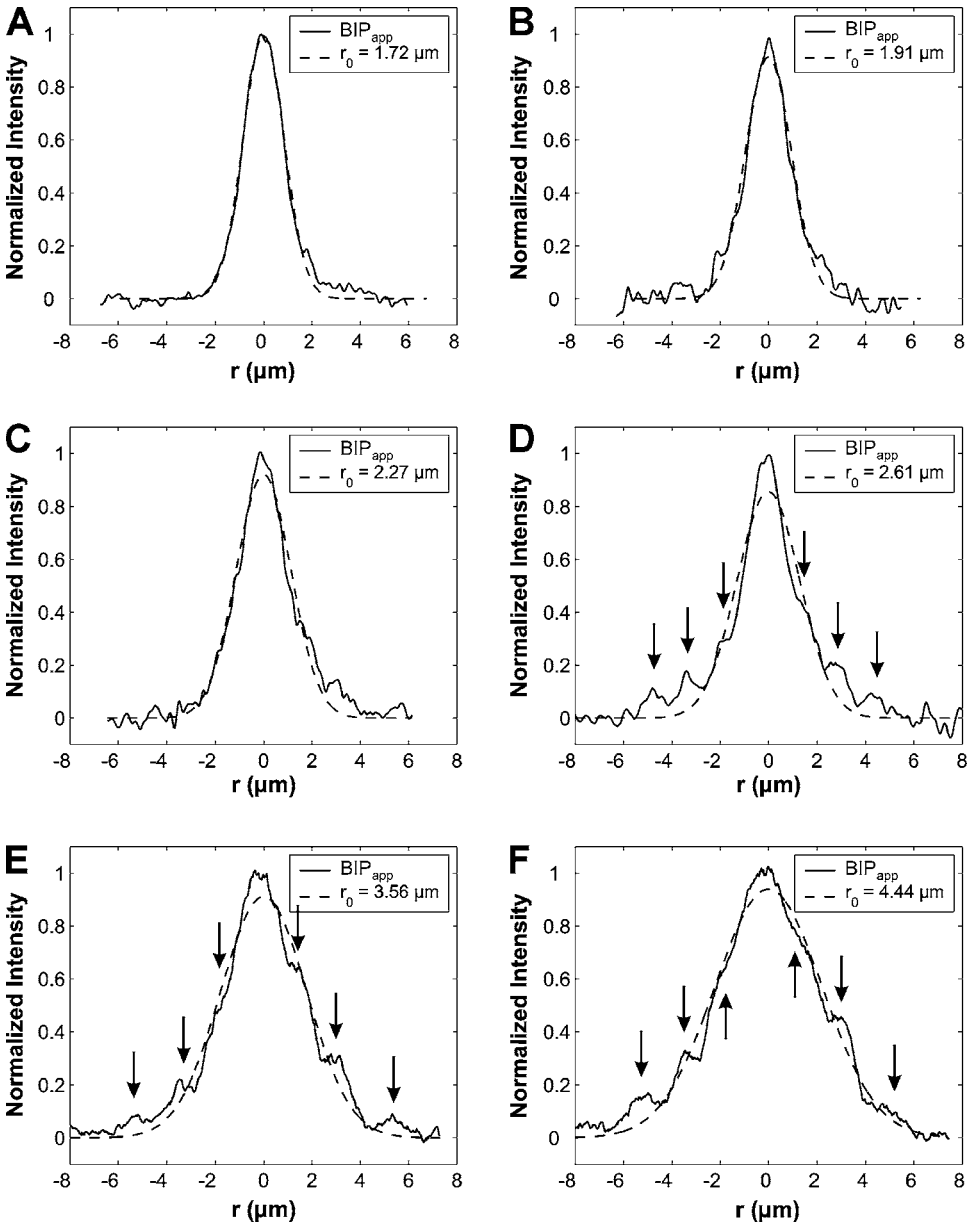

Fig. 4 The apparent BID in case of fluorescein depends on the specific bleaching conditions. (a) At a low bleaching intensity of 2 μW, only the central peak of the diffraction pattern effectively takes part in the bleaching process. Hence, the apparent BID corresponds to a Gaussian distribution. (b) At 10 mW and 25 μs bleach time, the apparent BID can still be approximated by a Gaussian distribution, although an expansion is already observed. (c) For a bleaching time of 50 μs, the apparent BID expands even more and (d) for 100 μs, the individual diffraction rings are becoming visible as indicated by the arrows. (e) Bleaching for 500 μs and (f) 1000 μs increases the relative contribution of the higher-order diffraction rings even more, causing a substantial expansion of the original BID.

have to take into account to explain the experimentally observed bleaching profile if the bleaching process would follow first-order kinetics. In other words, the "apparent BID" is the intensity distribution I_{app} that has to be used in Eq. (2) to correctly calculate the observed real bleaching profile. In case first-order photobleaching is valid, I_{app} should be identical to the intensity distribution as shown in Fig. 2(a). In the experiments below we will examine if this is true or not under a variety of photobleaching conditions. If C_b denotes the fluorescence concentration distribution after photobleaching, the normalized "apparent BID" can be calculated from

$$\frac{I_{app}(r)}{I_{app}(0)} = \frac{\ln(C_b(r)/C_0)}{\ln(C_b(0)/C_0)}. \tag{10}$$

The first spot (Fig. 3(a)) was bleached at a low intensity of 2 μW, which is typical for confocal imaging conditions, and a bleaching time of 125 ms. The apparent BID calculated from Fig. 3(a) using Eq. (10) is shown in Fig. 4(a). A best fit of Eq. (9) shows there is a very good correspondence of the apparent BID with a Gaussian intensity profile, in accordance with what is assumed theoretically in the FRAP models. We note that the bleached spot was not perfectly circular but was

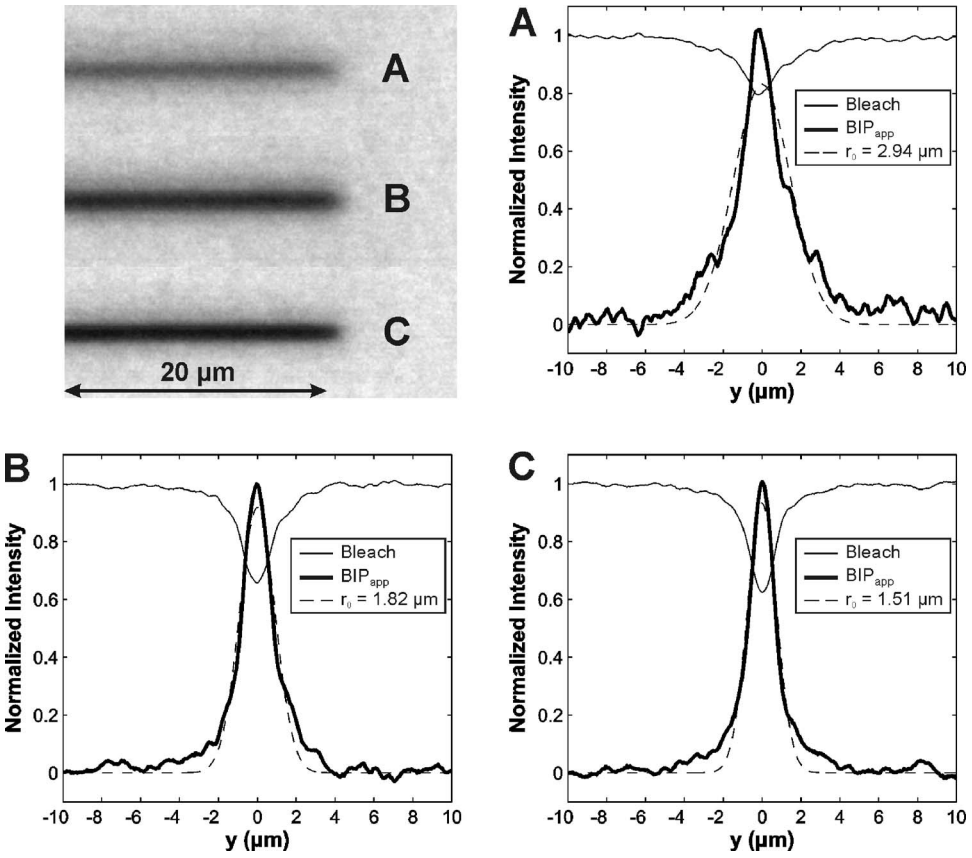

Fig. 5 Three line segments are photobleached at different bleaching intensities but with an equal total amount of light received. (a) Scanning twice at 10 mW, (b) 20 times at 1 mW, and (c) 267 times at 0.075 mW results each time in a different bleaching profile. Although all lines have received the same amount of light, bleaching is most efficient when scanning multiple times at a lower laser intensity. Bleaching at low intensities has the additional advantage of preserving a Gaussian distribution for the apparent BID, while an expansion is observed at high intensity levels.

stretched along the y-direction resulting in a slightly increased Gaussian radius. This is probably caused by a small difference in resolution in x and y because of the polarized laser light.[37] To check the validity of a Gaussian BID for high-intensity laser beams, spots were bleached at 10 mW and different bleaching times: 25 μs (image not shown), 50 μs (image not shown), 100 μs (Fig. 3(b)), 500 μs (Fig. 3(c)), 1000 μs (Fig. 3(d)), and 100 ms (Fig. 3(e)). A Gaussian apparent BID is still found for very short bleaching pulses of 25 μs (Fig. 4(b)) and 50 μs (Fig. 4(c)), although a slight broadening of the profile is already observed compared to Fig. 4(a). When bleaching for 100 μs (Fig. 4(d)), the higher-order diffraction rings are already starting to show up as indicated by the arrows and the corresponding apparent BID starts to deviate from a pure Gaussian distribution. For bleaching times of 500 μs (Fig. 4(e)) and 1000 μs (Fig. 4(f)) the higher-order diffraction rings become much more pronounced, expanding the apparent BID even more. Although the apparent BIDs do no longer correspond to a simple Gaussian distribution, it is worth noting that it is still possible to roughly approximate the apparent BIDs by an (expanded) Gaussian intensity distribution. Figure 3(e), finally, shows the situation if the bleaching time is prolonged to 100 ms. Besides the fourth-order diffraction ring, all kinds of diffraction spots take part in the bleaching process. Fitting of a Gaussian intensity distribution to the apparent BID in this case (data not shown) yielded a highly increased Gaussian resolution of r_0=7.6 μm. These experiments clearly show that the bleaching profiles obtained at high laser powers cannot be explained by first-order photobleaching alone. Assuming first-order kinetics leads to an *apparently* variable BID, which physically is nonsense. In reality, a higher laser power results in a higher amplitude of the BID but cannot change the shape of the distribution.

Besides being dependent on the bleaching time, the apparent BID also depends on the bleaching intensity. Since many FRAP techniques make use of a scanning beam for bleaching, a line photobleaching experiment instead of spot photobleaching was chosen here to explicitly show that the results from this study equally apply to a scanning beam as well. Three line segments of 80 μm are bleached at different bleaching powers, but with an equal total amount of light received. A first line is bleached by scanning two times at 10 mW. A second one is bleached at 1 mW by scanning 20 times. A third one is bleached at 75 μW by scanning 267 times. A confocal image of the right part of each of the line segments is shown in Fig. 5. The fluorescence intensity profile (along the y-direction) and the corresponding apparent BID are shown for each line in Figs. 5(a)–5(c). Assuming first-order bleaching kinetics, the bleaching profile of a single line segment [a, b] can be calculated from Eq. (3) with Δy=1 and $K(x,y,z) = \int_a^b I_b(x-x',y,z)dx'$.[11] For a Gaussian BID according to Eq. (9) and a line segment that is much longer than the resolution

r_0, the resulting bleaching intensity distribution finally becomes

$$K(x,y,z) = \sqrt{\frac{\pi}{2}} I_{0b} r_0 e^{-2y^2/r_0^2}. \quad (11)$$

Equation (11) expresses that, when scanning a Gaussian intensity beam along the x-direction, the Gaussian intensity distribution is preserved along the y-direction. Hence, if the bleaching process follows first-order kinetics, the apparent BID calculated from Eq. (10) should still be Gaussian-distributed with a resolution r_0 equal to that of the scanning beam. At a low bleaching intensity, the apparent BID is indeed Gaussian distributed (Fig. 5(c)), while a deviation from a pure Gaussian distribution occurs for increasing bleaching intensities (Figs. 5(b) and 5(a)). Fitting of a Gaussian intensity distribution in Fig. 5 explicitly shows the expansion of the apparent BIDs with increasing bleaching intensity. From the spot photobleaching experiments we already know that the expansion is mainly due to the participation of the higher-order diffraction rings in the non-first-order bleaching process. The individual diffraction maxima are difficult to distinguish, however, because of the scanning process along the x-direction. Additionally, it is clear from Fig. 5 that the amount of bleaching is different for each of the three situations as well, although all lines did receive an equal amount of light. Bleaching at high intensities for a short time appears to be less efficient than bleaching at lower intensities for a longer time.

4.2 *Simulation of Photobleaching Immobilized Fluorescein*

The photochemical reactions according to Table 1 and the corresponding mathematical model Eq. (7) can be used to explain the observations of the previous section. We will show that the expansion of the bleaching profiles—which is unexpected from classical FRAP models, which use first-order photobleaching to calculate the bleaching profile—can indeed be explained by the complex photobleaching reactions of fluorescein in combination with the very high laser powers that are used for the bleaching phase of an FRAP experiment. We note that, as most of the FITC-dextrans are immobilized in the acrylamide gel, the contribution of the D-D interactions to the bleaching of fluorescein is expected to be very small and virtually all bleaching will be due to the D-O reactions. This can be taken into account in the simulations by setting the rate constants k_2, k_3, k_4, k_5, k_6, and k_7 to zero. The initial concentration of fluorescein in the gel was approximately 250 μM (which can be calculated from the concentration of FD2000 in the gel and the loading degree of fluorescein on the dextran chains). The initial oxygen concentration is taken to be 250 μM as well.[25] Assuming that all fluorescein molecules are initially in the ground state, the simulations therefore always start from the initial condition: $N_S = 250$ μM, $N_{O_2} = 250$ μM, and $N_{S^*} = N_{T^*} = N_X = N_R = 0$.

We simulated the photobleaching of immobilized fluorescein as a function of time first to examine the evolution of the photobleaching process. The solid lines in Fig. 6 are calculated for a bleaching intensity of 10 mW and a bleaching time of 1 ms. From 10^{-11} s on, the ground state S is being depleted

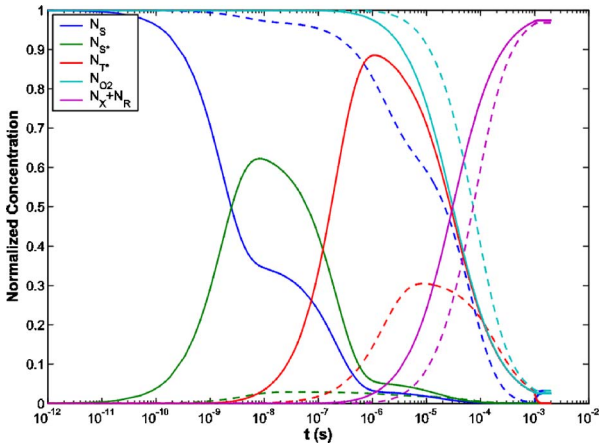

Fig. 6 The evolution over time of fluorescein molecules in the various energy levels is simulated for an illumination intensity of 10 mW (solid lines) and 0.17 mW (dashed lines). The evolution of the number of oxygen molecules and the photobleaching products is shown as well. All populations are normalized to the initial fluorophore population at the ground state. The bleaching time is 1 ms, after which the illumination is switched off ($k_a = 0$) and the reactions are allowed to continue until all fluorescein molecules are photobleached or back in the ground state.

to the advantage of the excited singlet state S^* that peaks at around 10^{-8} s. After 10^{-8} s, the excited singlet state S^* starts to decay to both the ground state S and the long-lived excited triplet state T^*. Between 10^{-8} and 10^{-6} s, almost all fluorescein molecules are gradually getting trapped in the long-lived excited triplet state T^*. Once the triplet state population starts to rise, the D-O reactions can start producing the photobleaching products X and R, which are formed from 10^{-7} s on. The formation of the photobleaching products X and R cause the triplet state to be depleted, together with the number of oxygen molecules. At 10^{-4} s, almost no molecules are left in the ground state because all are either photobleached or in the triplet state. At 10^{-3} s, the illumination is switched off ($k_a = 0$) and the reactions are allowed to continue until all molecules are either photobleached or back in the ground state.

The first-order maximum of the BID has a relative intensity of 1.7% (see Fig. 2(b)). To see what happens at this intensity level, the same calculations were repeated at a bleaching power of 0.17 mW (Fig. 6, dashed lines). Essentially the same processes are taking place, albeit somewhat delayed because of the reduced illumination intensity. It is important to note that the triplet state still becomes significantly populated to approximately 30%, despite the very much reduced illumination intensity. As a result, about the same level of bleaching is reached after 10^{-3} s, which explains why the higher-order diffraction rings are showing up in the bleaching experiments.

To see this more clearly, calculations have been performed for a BID according to Eq. (8) (also see Fig. 2(b)) at a bleaching power of 10 mW and for different bleaching times. Figure 7(a) shows the result for $t = 25$ μs. The apparent BID is again calculated from the bleaching profile using Eq. (10). For comparison with the experimental data (Fig. 4(b)), it should be realized that the simulated bleaching profile is not what is observed directly through a microscope. When observing an object through a microscope, it is modulated by the micro-

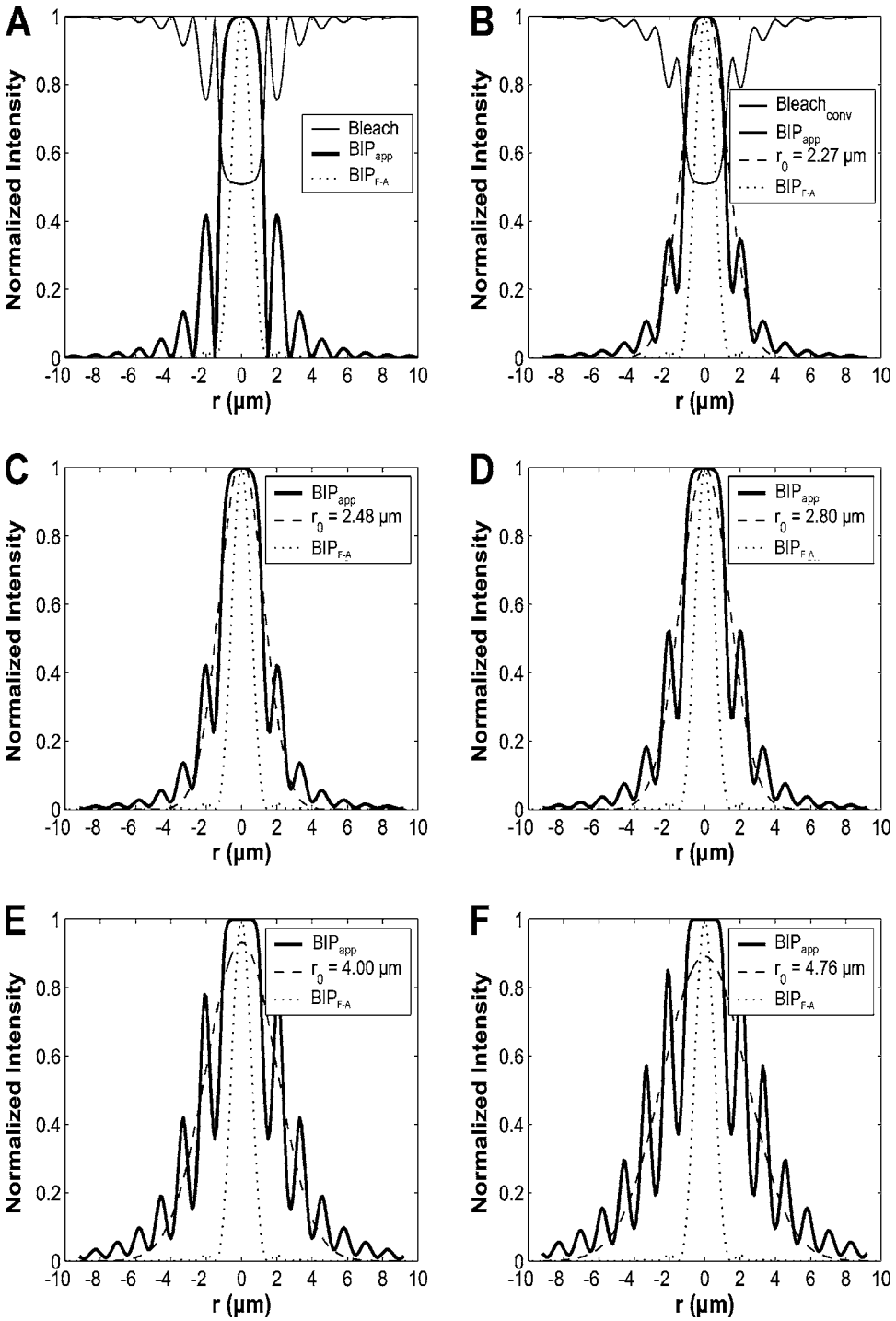

Fig. 7 The bleaching of immobilized fluorescein by a stationary laser beam is simulated for a laser power of 10 mW and different bleaching times. The dotted line shows the intensity distribution of the illumination BID according to the Fraunhofer–Airy formula [Eq. (8)] for a resolution of 1.5 μm. (a) The solid line shows the bleaching profile for $t=25$ μs. The bold line is the corresponding apparent BID. (b) When an object is observed by a microscope, it is modulated by the total PSF, which depends primarily on the objective lens that is used. The results of (a) are therefore convolved with a Gaussian mask having a resolution radius of 0.2 μm in accordance with the properties of the 60× objective lens used in the experimental section. As a result, the individual maxima appear less pronounced. The dashed line is a best fit of a Gaussian intensity distribution to the apparent BID. The fitted Gaussian resolution is specified in the legend. (c–f) The same calculations are repeated for bleaching times of 50 μs, 100 μs, 500 μs, and 1000 μs. The longer the bleaching time, the more the higher-order diffraction maxima contribute to the apparent BID. As a result, the apparent BID expands with increasing bleaching time.

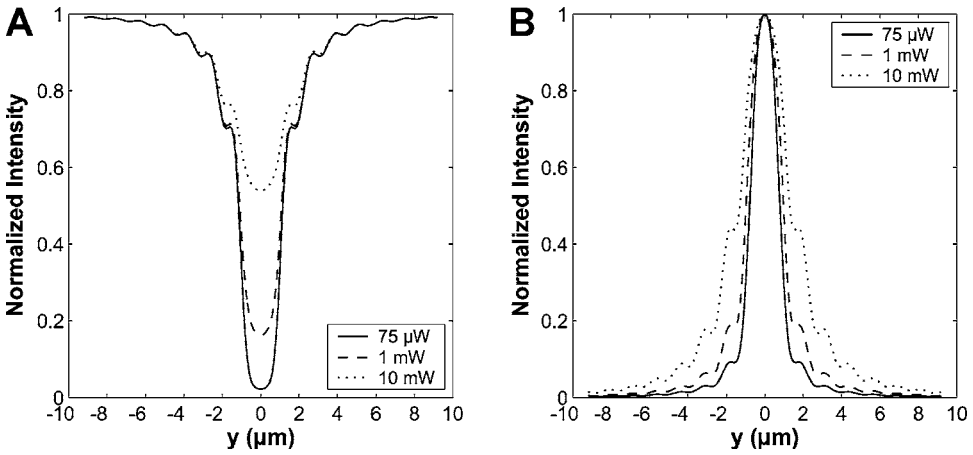

Fig. 8 The bleaching of three lines is simulated for three different intensities: 75 μW, 1 mW, and 10 mW. To obtain the same total amount of light for each of the lines, the scanning speed is changed accordingly. (a) The bleaching profiles show that a better bleaching efficiency is obtained when using a low power beam in combination with a reduced scanning speed. (b) From the corresponding apparent BIDs it is clear that at high intensities the higher-order diffraction maxima are able to contribute significantly to the bleaching process. As a result, the apparent BID expands with increasing bleaching intensity.

scope's total point spread function (PSF), which depends directly on the objective lens being used.[29,38] The detection PSF of an objective lens in the focal plane of a confocal microscope can be approximated by a Gaussian intensity distribution corresponding to the central diffraction peak. This is allowed because the higher-order diffraction rings only have a small contribution to the collected fluorescence compared to the central peak and because the higher-order diffraction rings are largely blocked by the small confocal apperture (see, e.g., Fig. 2 of Jonkman and Keller[29]). The 60× objective lens used to image the bleaching profiles has a Gaussian resolution r_0 of approximately 0.2 μm. To obtain a more direct comparison between the simulated and experimental data, the simulated bleaching profile is therefore convolved with a corresponding Gaussian mask. The result is shown in Fig. 7(b). The individual maxima seem less pronounced because of the limited resolving power of the objective lens. Together with the presence of noise, this explains why the individual maxima are not always easy to discern in the experimental apparent BIDs (compare with Fig. 4). The same calculations have been performed for t=50 μs (Fig. 7(c)), 100 μs (Fig. 7(d)), 500 μs (Fig. 7(e)), and 1000 μs (Fig. 7(f)). Only the convolved apparent BIDs together with a Gaussian fit are shown for clarity. Comparing Figs. 4(b)–4(f) with Figs. 7(b)–7(f) shows that the theory corresponds well with what is observed experimentally: an apparent BID that expands with increasing bleaching time due to the increasing contribution to the bleaching process of the higher-order diffraction rings. Again we find that each of the expanded apparent BIDs can roughly be approximated by a Gaussian distribution.

It is worth noting that the simulation results not only correspond qualitatively to the experimental observations, but that there is also a reasonable quantitative correspondence between both. The simulation parameters used to obtain the results from Fig. 7 were chosen thus to directly reflect the experimental conditions leading to the results presented in Fig. 4. Figure 7(b) is in fact the simulation of the experiment in Figs. 4(b) and 7(c) is the simulation of 4c and so on (the experiment of Fig. 4(a) was not simulated). In all cases a Gaussian distribution was fitted to the apparent BID to quantify the expansion through the Gaussian resolution parameter r_0. The values for r_0 are reported in each of the figures, from which it can be seen that there is a fairly good correspondence between the experimental and simulated values. The simulated results deviate from the experimental ones only by 19%, 9%, 7%, 12%, and 7% for the Figs. 7(b)–7(f), respectively. This further supports the validity of the model being used and the accuracy of the computations presented here.

The line photobleaching experiments have been simulated as well for bleaching powers of 10 mW, 1 mW, and 0.075 mW. The simulation program does not allow us to calculate repeated line scans because of the extensive computation times involved. Alternatively we have simulated line profiles using those three intensities but with different scanning speeds. The scanning speed at 1 mW was 1/10 of the scanning speed at 10 mW, and 1/133 at 0.075 mW. Hence, the same amount of light will be received in all three cases. The resulting bleaching profiles are shown in Fig. 8(a). In correspondence with the experimental observations, a better bleaching efficiency is obtained when using a low bleaching intensity with an increased bleaching time. This effect can be explained as follows. The high-intensity beam quickly depletes the ground state in favor of the triplet state, which will soon become saturated. The low-intensity beam, on the other hand, will only partly populate the triplet state at any one time, but integrated over the entire time span a larger number of triplet states will have existed, effectively leading to a larger number of photobleached molecules. Although in both cases an identical total amount of light dose was received, the lower light intensity applied for an extended period of time effectively causes more bleaching than the short saturating high-intensity bleach pulse. The apparent BIDs are shown in Fig. 8(b). Again we find an expansion of the apparent BID with increasing bleaching intensities. Fitting of a Gaussian distribution to the simulated profiles (not shown in Fig. 8(b)) gives r_0-values of 1.32 μm, 1.72 μm, and 2.95 μm for the bleaching powers of 75 μW, 1 mW, and 10 mW, respec-

tively. As indicated in Fig. 5, the experimental r_0-values are (in the same order) 1.51 μm, 1.82 μm, and 2.94 μm. Thus we obtain a deviation of the simulated from the experimental results of 13%, 6%, and 0%. Again we find a good quantitative correspondence between the simulated and experimental results.

5 Discussion

Both theory and experiments confirm that generally the photobleaching of fluorescein does not follow a simple exponential decay. This is especially the case for typical bleaching conditions of a FRAP experiment where high-intensity light levels are used for very fast photobleaching and cause saturation of fluorescein in the triplet excited state. We have demonstrated that under those conditions it is no longer sufficient to solely take the central diffraction spot into account as is assumed in the derivation of many FRAP models. Instead it has become clear that the higher-order diffraction rings can induce a significant amount of photobleaching, mainly due to the saturation of the fluorophore in the long-lived triplet state from which the bleaching actually proceeds. The net result is an *apparent* bleaching illumination intensity distribution that is expanded with regard to the *actual* bleaching illumination intensity distribution. In addition, not only does the apparent BID depend on the bleaching intensity, it also depends on the bleaching time or scanning speed in case of a stationary or scanning beam, respectively.

We have shown by simulations and experiments that the actual situation is even more complicated. Besides being dependent on the different illumination parameters, the photobleaching of fluorescein is also dependent on multiple photochemical reactions, as summarized in Table 1. The individual reaction rates of the D-D and D-O reactions will, for example, depend on the mobility of the respective molecules in the system. The values reported in Table 1 are for free fluorescein in solution, but may be different when fluorescein is present in actual samples, such as cells or biopolymer gels. As a result, the various reaction rates will depend on the sample under study. It is also likely that in complex chemical systems, such as an intracellular environment, additional reactions will take part in the photobleaching process of fluorescein. Moreover, the bleaching process also depends on the molar concentrations of both fluorescein and oxygen in the system. Considering the variability of these parameters, whose exact values are unknown in most cases, it becomes clear that the apparent BID cannot be accurately predicted for actual experiments.

FRAP models almost always assume first-order photobleaching kinetics. Hence the concentration distribution after bleaching can be calculated directly from a single exponential function [Eq. (2) or Eq. (3)] and an invariant Gaussian BID [Eq. (9)], which is solely determined by the microscope optics. For fluorescein we have demonstrated that, when assuming first-order kinetics, the BID can no longer be considered to be invariant. Instead an "apparent BID" had to be defined whose shape and intensity depends on many parameters. We have also shown that the apparent BID can be roughly approximated by a Gaussian intensity distribution whose resolution will depend on the specific experimental conditions. It is therefore to be expected that existing FRAP models are still able to calculate valid diffusion coefficients from experiments under saturating conditions, as long as the correct apparent Gaussian resolution can be determined for every single experiment. If not, serious errors will result. For example, in the FRAP equation for spot photobleaching with a Gaussian beam in the fundamental work of Axelrod,[12] the diffusion coefficient D is calculated from fitting the parameter D/r_0^2 to the experimental recovery curve, where r_0 is the Gaussian resolution of the bleaching beam. Hence the resolution r_0 has to be known with great precision to obtain an accurate diffusion coefficient. Our experiments have shown that an expansion of the apparent Gaussian radius with a factor 2 to 5 is very well possible. If one does not take this effect into account, the calculated diffusion coefficient would consequently be erroneous by a factor 4 to 25. We note that broadening of the bleach area can also occur when using bleach times that are too long, in which case diffusion will occur during bleaching. Most FRAP models assume an instantaneous photobleaching phase, i.e., no diffusion during bleaching. While long bleach times will lead to the similar result of bleach area broadening, the "anomalous" photobleaching discussed in this study is really of a different nature and is inherent to the fluorophore photobleaching mechanism. Diffusion during bleaching, on the other hand, can simply be avoided by understanding the FRAP model being used and carrying out the experiments accordingly.

There are a few possibilities to deal with a variable apparent BID. For FRAP models that explicitly require the knowledge of the Gaussian resolution r_0, the most direct solution in this case is to extract r_0 directly from the experiments, which can be done by acquiring an image of the bleaching profile immediately after the bleaching phase (which is independent of D) and using the FRAP formula to extract r_0. In practice it is difficult, however, to obtain an image immediately after bleaching because of limited image acquisition rates. Even then most FRAP models would need an adjustment of the theory to take a different bleaching and illumination distribution into account.

A workaround is to use FRAP models that do not require the precise knowledge of the BID or the concentration distribution after bleaching. Examples are the models that use the Fourier transform of the recovery images.[39–41] They have shown that the diffusion coefficient can be calculated without determining the BID of the microscope by measuring the decay of the spatial Fourier transform of the recovery images. Another example is the model of Kubitscheck et al.,[33] who have derived a moment's analysis of the fluorescence recovery images that does not require the knowledge of the initial concentration distribution after bleaching. The results from this study suggest that methods using a relative determination of the diffusion coefficient[3,42] should be used with care in case of fluorescent dyes with a complex bleaching mechanism, such as fluorescein. Such a method relies on two series of FRAP experiments, one in the actual sample and one in a series of standard solutions of known viscosity. If both FRAP experiments are performed under exactly the same conditions, the diffusion coefficient in the sample can be calculated relative to the calibration reference solutions without knowing the actual bleaching profile. This approach could lead to invalid results because the reaction rates, and hence the apparent

BID, depend directly on the mobility of the molecules that take part in the bleaching process. For example, in a gel system with small interstitial spaces, larger molecules such as FITC-dextrans can experience a strongly reduced diffusion coefficient due to sterical hindrance, while the smaller oxygen molecules can still diffuse as rapidly as in solution. Consequently, the dye-dye reaction constants k_{2-7} (see Table 1) will have a lower value in the gel system as compared to in solution, leading to a change in the photobleaching process and hence in the apparent BID. Therefore, even under the exact same illumination conditions, the bleaching profile in the sample will, in general, be different from the one in solution, and consequently a general relation between the two recovery curves may not be possible any more.

An alternative is to use a FRAP model where an area is uniformly bleached that is much larger than the characteristic dimensions of the BID. Recently, we derived such a model for use with the confocal microscope based on the bleaching of a uniform disk having a radius of at least 4 times the Gaussian resolution of the apparent BID.[11] In that case, a change of the shape of the BID will only be "felt" at the boundaries of the bleached area. We have shown that neglecting the expansion of the BID usually will not cause errors larger than 10% in the determination of the diffusion coefficient. Hence this method can be used with great confidence and does not require special measures.

The most straightforward solution is, of course, to avoid fluorescent dyes that easily saturate. From experience we know that one such fluorophore is NODD (N-(7-nitrobenz-2-oxa-1,3-diazol-4-yl)diethyl amine). NODD is incorporated in polystyrene microspheres that are encoded by photobleaching.[31,43] In this application it is essential to have the best possible resolution (i.e., a non-expanded BID) to write as much information as possible per unit area. It needs to be examined, though, which other fluorophores for FRAP meet this condition as well. This could be done, for example, by performing FRAP experiments on a series of samples with a known diffusion coefficient. If the diffusion coefficient is known, the apparent Gaussian resolution r_0 for each of the solutions can be calculated from the corresponding FRAP formula. If r_0 remains constant for all samples, the apparent BID is invariant for that particular fluorophore and is suitable for use with the existing FRAP models. We are currently developing a new FRAP model for use with the confocal microscope based on the bleaching of a line segment taking both an independent bleaching and imaging illumination intensity distribution into account. This model will be very well suited to characterize the expansion of the apparent BID—in terms of the Gaussian resolution r_0—as a function of the bleaching intensity and duration for different kinds of fluorophores. It would especially be interesting to do this for GFP and its variants, which are popular fluorophores for intracellular FRAP experiments.

Finally, we note that our bleaching experiments and simulations have shown that the change in shape of the BID is small when using a low-power bleaching beam (in combination with an extended bleaching time). Because most FRAP models assume a very short bleaching phase t_b compared to the characteristic recovery time τ ($t_b < 0.15\tau$), this approach will only offer a solution in case of sufficiently slow diffusion.

6 Conclusions

In this study we have examined the effect of excitation saturation on FRAP experiments. As a case study we have looked in detail at the photochemical bleaching reactions of fluorescein, one of the most frequently used fluorophores for FRAP. We have presented both experimental and theoretical evidence that, mainly due to saturation of the triplet excited state, the basic assumptions that are made in many FRAP models are generally no longer valid: an invariant bleaching illumination intensity distribution in combination with first-order photobleaching kinetics. Instead, saturation leads to a dramatically variable apparent bleaching illumination intensity distribution. This effect is not always immediately evident from the experiments, but neglecting it can induce errors of more than one order of magnitude in the calculation of the diffusion coefficient. Therefore, it seems advisable to look for photobleachable fluorophores that do not as easily saturate or to use/develop FRAP models that are insensitive to the actual shape of the bleaching illumination intensity distribution.

Acknowledgments

The financial support of the IWT is acknowledged with gratitude. Ghent University (BOF) is acknowledged for its support through instrumentation credits. Kevin Braeckmans is a Postdoctoral Fellow of the Fund for Scientific Research–Flanders (Belgium).

References

1. T. K. L. Meyvis, S. C. De Smedt, P. Van Oostveldt, and J. Demeester, "Fluorescence recovery after photobleaching: A versatile tool for mobility and interaction measurements in pharmaceutical research," *Pharm. Res.* **16**(8), 1153–1162 (1999).
2. J. G. McNally and H. Smith, "Photobleaching by confocal microscopy," Chap. 25 in *Confocal and Two-Photon Microscopy*, A. Diaspro, Ed., pp. 525–538, Wiley-Liss, New York (2002).
3. A. S. Verkman, "Diffusion in cells measured by fluorescence recovery after photobleaching," *Biophotonics, Part A: Methods in Enzymology*, G. Marriott and I. Parker, Eds., pp. 635–648, Academic Press, New York (2003).
4. M. Edidin, "Translational diffusion of membrane proteins," *The Structure of Biological Membranes*, P. Yeagle, Ed., pp. 539–572, CRC Press, Boca Raton, Fla (1992).
5. A. Ishihara and K. Jacobson, "A closer look at how membrane-proteins move," *Biophys. J.* **65**(5), 1754–1755 (1993).
6. O. Seksek, J. Biwersi, and A. S. Verkman, "Translational diffusion of macromolecule-sized solutes in cytoplasm and nucleus," *J. Cell Biol.* **138**(1), 131–142 (1997).
7. F. Umenishi, J. M. Verbavatz, and A. S. Verkman, "cAMP regulated membrane diffusion of a green fluorescent protein-aquaporin 2 chimera," *Biophys. J.* **78**(2), 1024–1035 (2000).
8. W. M. Saltzman, M. L. Radomsky, K. J. Whaley, and R. A. Cone, "Antibody diffusion in human cervical-mucus," *Biophys. J.* **66**(2), 508–515 (1994).
9. S. S. Olmsted, J. L. Padgett, A. I. Yudin, K. J. Whaley, T. R. Moench, and R. A. Cone, "Diffusion of macromolecules and virus-like particles in human cervical mucus," *Biophys. J.* **81**(4), 1930–1937 (2001).
10. N. N. Sanders, S. C. De Smedt, and J. Demeester, "The physical properties of biogels and their permeability for macromolecular drugs and colloidal drug carriers," *J. Pharm. Sci.* **89**(7), 835–849 (2000).
11. K. Braeckmans, L. Peeters, N. N. Sanders, S. C. De Smedt, and J. Demeester, "Three-dimensional fluorescence recovery after photobleaching with the confocal scanning laser microscope," *Biophys. J.* **85**(4), 2240–2252 (2003).
12. D. Axelrod, D. E. Koppel, J. Schlessinger, E. Elson, and W. W. Webb, "Mobility measurement by analysis of fluorescence photobleaching recovery kinetics," *Biophys. J.* **16**(9), 1055–1069 (1976).
13. D. M. Soumpasis, "Theoretical-analysis of fluorescence photobleach-

ing recovery experiments," *Biophys. J.* **41**(1), 95–97 (1983).
14. A. Lopez, L. Dupou, A. Altibelli, J. Trotard, and J. F. Tocanne, "Fluorescence recovery after photobleaching (FRAP) experiments under conditions of uniform disk illumination—critical comparison of analytical solutions, and a new mathematical method for calculation of diffusion coefficient-D," *Biophys. J.* **53**(6), 963–970 (1988).
15. J. C. G. Blonk, A. Don, H. Van Aalst, and J. J. Birmingham, "Fluorescence photobleaching recovery in the confocal scanning light-microscope," *J. Microsc.* **169**, 363–374 (1993).
16. G. W. Gordon, B. Chazotte, X. F. Wang, and B. Herman, "Analysis of simulated and experimental fluorescence recovery after photobleaching—data for 2 diffusing components," *Biophys. J.* **68**(3), 766–778 (1995).
17. P. Wedekind, U. Kubitscheck, O. Heinrich, and R. Peters, "Line-scanning microphotolysis for diffraction-limited measurements of lateral diffusion," *Biophys. J.* **71**(3), 1621–1632 (1996).
18. T. J. Feder, I. BrustMascher, J. P. Slattery, B. Baird, and W. W. Webb, "Constrained diffusion or immobile fraction on cell surfaces: A new interpretation," *Biophys. J.* **70**(6), 2767–2773 (1996).
19. Y. Cheng, R. K. Prud'homme, and J. L. Thomas, "Diffusion of mesoscopic probes in aqueous polymer solutions measured by fluorescence recovery after photobleaching," *Macromolecules* **35**(21), 8111–8121 (2002).
20. G. Carrero, D. McDonald, E. Crawford, G. de Vries, and M. J. Hendzel, "Using FRAP and mathematical modeling to determine the in vivo kinetics of nuclear proteins," *Methods* **29**(1), 14–28 (2003).
21. L. S. Cutts, P. A. Robberts, J. Adler, M. C. Davies, and C. D. Melia, "Determination of localized diffusion-coefficients in gels using confocal scanning laser microscopy," *J. Microsc.* **180**, 131–139 (1995).
22. C. Dietrich, R. Merkel, and R. Tampe, "Diffusion measurement of fluorescence-labeled amphiphilic molecules with a standard fluorescence microscope," *Biophys. J.* **72**(4), 1701–1710 (1997).
23. U. Kubitscheck, P. Wedekind, and R. Peters, "Three-dimensional diffusion measurements by scanning microphotolysis," *J. Microsc.* **192**, 126–138 (1998).
24. J. Crank, *The Mathematics of Diffusion*, Clarendon Press, Oxford, UK (1975).
25. L. L. Song, E. J. Hennink, I. T. Young, and H. J. Tanke, "Photobleaching kinetics of fluorescein in quantitative fluorescence microscopy," *Biophys. J.* **68**(6), 2588–2600 (1995).
26. R. Y. Tsien and A. Waggoner, "Fluorophores for confocal microscopy," *Handbook of Biological Confocal Microscopy*, J. B. Pawley, Ed., pp. 267–279, Plenum Press, New York (1995).
27. K. D. Mielenz, "On the diffraction limit for lensless imaging," *J. Res. Natl. Inst. Stand. Technol.* **104**(5), 479–485 (1999).
28. M. Born and E. Wolf, *Principles of Optics*, Cambridge University Press, Cambridge, UK (1999).
29. J. E. N. Jonkman and E. H. K. Stelzer, "Resolution and contrast in confocal and two-photon microscopy," Chap. 5 in *Confocal and Two-Photon Microscopy*, A. Diaspro, Ed., pp. 101–125, Wiley-Liss, New York (2002).
30. S. Inoué, "Foundations of confocal scanned imaging in light microscopy," Chap. 1 in *Handbook of Biological Confocal Microscopy*, J. B. Pawley, Ed., pp. 1–17, Plenum Press, New York (1995).
31. K. Braeckmans, S. C. De Smedt, C. Roelant, M. Leblans, R. Pauwels, and J. Demeester, "Encoding microcarriers by spatial selective photobleaching," *Nat. Mater.* **2**(3), 169–173 (2003).
32. P. Wedekind, U. Kubitscheck, and R. Peters, "Scanning microphotolysis—A new photobleaching technique based on fast intensity modulation of a scanned laser-beam and confocal imaging," *J. Microsc.* **176**, 23–33 (1994).
33. U. Kubitscheck, P. Wedekind, and R. Peters, "Lateral diffusion measurement at high-spatial-resolution by scanning microphotolysis in a confocal microscope," *Biophys. J.* **67**(3), 948–956 (1994).
34. P. Gribbon and T. E. Hardingham, "Macromolecular diffusion of biological polymers measured by confocal fluorescence recovery after photobleaching," *Biophys. J.* **75**(2), 1032–1039 (1998).
35. Y. Cheng, R. K. Prud'homme, and J. L. Thomas, "Diffusion of mesoscopic probes in aqueous polymer solutions measured by fluorescence recovery after photobleaching," *Macromolecules* **35**(21), 8111–8121 (2002).
36. G. Carrero, D. McDonald, E. Crawford, G. de Vries, and M. J. Hendzel, "Using FRAP and mathematical modeling to determine the in vivo kinetics of nuclear proteins," *Methods* **29**(1), 14–28 (2003).
37. C. J. Cogswell and K. G. Larkin, "The specimen illumination path and its effect on image quality," Chap. 8 in *Handbook of Biological Confocal Microscopy*, J. B. Pawley, Ed., pp. 127–137, Plenum Press, New York (1995).
38. P. J. Shaw, "Comparison of wide-field deconvolution and confocal microscopy for 3D imaging," Chap. 23 in *Handbook of Biological Confocal Microscopy*, J. B. Pawley, Ed., pp. 373–387, Plenum Press, New York (1995).
39. T. T. Tsay and K. A. Jacobson, "Spatial Fourier-analysis of video photobleaching measurements—principles and optimization," *Biophys. J.* **60**(2), 360–368 (1991).
40. D. A. Berk, F. Yuan, M. Leunig, and R. K. Jain, "Fluorescence photobleaching with spatial Fourier-analysis—measurement of diffusion in light-scattering media," *Biophys. J.* **65**(6), 2428–2436 (1993).
41. A. E. Cowan, D. E. Koppel, B. Setlow, and P. Setlow, "A soluble protein is immobile in dormant spores of Bacillus subtilis but is mobile in germinated spores: Implications for spore dormancy," *Proc. Natl. Acad. Sci. U.S.A.* **100**(7), 4209–4214 (2003).
42. H. P. Kao, J. R. Abney, and A. S. Verkman, "Determinants of the translational mobility of a small solute in cell cytoplasm," *J. Cell Biol.* **120**(1), 175–184 (1993).
43. K. Braeckmans, S. C. De Smedt, M. Leblans, R. Pauwels, and J. Demeester, "Encoding microcarriers: Present and future technologies," *Nat. Rev. Drug Discovery* **1**(6), 447–456 (2002).